Spin Dynamics Investigation of Quasi-Frozen Spin Lattice for EDM Searches

Eremey Valetov,[1, 2, *] Yurij Senichev,[2] and Martin Berz[1]

(On behalf of the JEDI Collaboration)

[1] *Michigan State University, East Lansing, MI 48824, USA*
[2] *IKP, Forschungszentrum Jülich, Germany*

(Dated: September 27, 2016)

The Quasi-Frozen Spin (QFS) method was proposed by Yu. Senichev *et al.* in [1] as an alternative to the Frozen Spin (FS) method for the search of deuteron electric dipole moment (dEDM). The QFS approach simplifies the design of the lattice. In particular, small changes to the currently operating COSY storage ring will satisfy the QFS condition. Spin decoherence and systematic errors fundamentally limit EDM signal detection and measurement. Our QFS implementation method includes measurement of spin precession in (1) the horizontal plane to calibrate the magnetic field when changing field polarity and (2) the vertical plane to search for EDM. To address systematic errors due to element misalignments, we track particle bunches in forward and reverse directions. We have modeled and tracked two QFS and one FS lattice in *COSY INFINITY*. The models include normally distributed random variate spin kicks in magnetic dipoles and in combined E and B field elements. We have used *Wolfram Mathematica* programs to partially automate lattice input file generation and tracking data analysis. We have observed additional indications that the QFS method is a viable alternative to the FS method.

I. INTRODUCTION

A. The Quasi-Frozen Spin Concept

The Frozen Spin (FS) concept for search of a deuteron electric dipole moment (dEDM) was proposed in the BNL Report [2]. The FS concept is based on the idea that (1) the spin vector is aligned with the particle momentum vector as the particle moves in a lattice and (2) the radial electrostatic field results in torque on the spin vector, rotating it out of the midplane.

The generalized Thomas-BMT equation is

$$\frac{d\vec{S}}{dt} = \vec{S} \times \left(\vec{\Omega}_{\mathrm{MDM}} + \vec{\Omega}_{\mathrm{EDM}} \right),$$

where the magnetic dipole moment (MDM) angular frequency is

$$\vec{\Omega}_{\mathrm{MDM}} = \frac{e}{m} \left[G\vec{B} - \left(G - \frac{1}{\gamma^2 - 1} \right) \frac{\vec{E} \times \vec{\beta}}{c} \right]$$

and the electric dipole moment (EDM) angular frequency is

$$\vec{\Omega}_{\mathrm{EDM}} = \frac{e}{m} \frac{\eta}{2} \left[\frac{\vec{E}}{c} + \vec{\beta} \times \vec{B} \right].$$

The Quasi-Frozen Spin (QFS) concept is based on the FS concept, but the requirement that spin needs to be aligned with momentum is relaxed: in QFS, spin is aligned with momentum *on average*. The QFS condition is expressed as

$$\gamma G \Phi_B = \left[\frac{1}{\gamma} (1 - G) + \gamma G \right] \Phi_E,$$

where Φ_B and Φ_E are the average angles of momentum rotation due to magnetic and electric fields, respectively.

In our spin decoherence and systematic errors studies concerning FS and QFS concepts, we consider three lattices codenamed *Senichev 6.3*, *Senichev E+B*, and *Senichev BNL*. Spin decoherence in these lattices is suppressed by the following:

1. RF cavity: first and, partially, second order by mixing the particles relatively to the average field strength, averaging out the $\triangle \gamma G$ for each particle.

2. Sextupoles: the remaining second order component, which is due to the average of $\triangle \gamma G$ being different for each particle.

B. Senichev FS and QFS Lattices

Senichev 6.3 QFS lattice [1] This lattice consists of 4 straight, 4 magnetic, and 4 electrostatic sections. It has the characteristic "hourglass" shape. A variation of this lattice can be implemented with relatively minor changes to a number of existing lattices, including the Cooler Synchrotron COSY at Forschungszentrum Jülich.

Senichev E+B QFS lattice [3] This lattice consists of 2 straight, 4 magnetic, and 2 straight E+B sections. The straight E+B static Wien filter elements are used instead of the curved electrostatic deflectors (1) to remove nonlinear components due to curvature in cylindrical electrostatic element electrodes and (2) to simplify the system from the engineering perspective.

Senichev BNL FS lattice This lattice consists of 2 straight and 2 curved E+B sections. The design of this lattice implements the FS method and is similar to the lattice described in the `RingLat` Appendix of [2]. The curved E+B sections use the curved E+B element proposed in [2].

---

* valetove@msu.edu

The straight sections in the lattices provide for the accelerating station, sextupoles, beam injection and extraction, and measurement equipment, including the polarimeter.

II.   COMPUTATIONAL METHODS

A.   Computational Software

We use *COSY INFINITY* 9.2 [4] for various spin tracking calculations, including:

1. the manual and automatic spin decoherence optimization by sextupole family strengths;

2. the investigation of spin decoherence growth as a function of the number of turns; and

3. the study of the effects of systematic errors on spin decoherence.

For the reader's convenience, we note that all calculations in *COSY INFINITY* are performed in, at the minimum, the following coordinates:

$$r_1 = x, \qquad\qquad r_2 = a = p_x/p_0,$$
$$r_3 = y, \qquad\qquad r_4 = b = p_y/p_0,$$
$$r_5 = l = -(t - t_0)\, v_0 \frac{\gamma}{1+\gamma}, \; r_6 = \delta_K = \frac{K - K_0}{K},$$
$$r_7 = \delta_m = (m - m_0)/m, \quad r_8 = \delta_z = (z - z_0)/z_0.$$

where x and y are local transversal spacial coordinates in meters; p, K, v, t, γ, m, and z are the momentum, kinetic energy, velocity, time of flight, total energy over mc^2, mass, and charge respectively; and the index 0 refers to the reference particle.

We use *Wolfram Mathematica* 10.4 for:

1. the automated preparation of *COSY INFINITY* input files from templates using markers and regular expressions; and

2. the storage, processing, quality assurance, and report generation using data from the *COSY INFINITY* output files.

B.   Spin Decoherence Optimization

We optimize the spin decoherence by sextupole strengths as follows:

1. We manually minimize spin decoherence up to $\pm 0.2\,\mathrm{T/m}$ by sextupole family strengths in the $x - a$, $y - b$, and $l - \delta_K$ planes with a set of RF cavity frequencies and voltages.

2. We completed the optimization automatically using the LMDIF optimizer that is built into *COSY INFINITY*. At optimal values, the sextupole family strength typically has a 10^{-3} T/m error without a significant impact on the spin decoherence.

C.   Reverse Spin Transfer Map

Since we track spin motion in lattices in both forward and reverse directions, we need to compute reverse orbital and spin transfer maps. There is already a built-in procedure for computation of the reverse orbital transfer map in *COSY INFINITY*. We have introduced a procedure to calculate the reverse spin transfer map in 2016.

Consider a spin transfer map $M : X_i \to X_{i+1}$, where both X_i and X_{i+1} are the 3D sphere S^3. Taking into account the nonlinear terms, M is a 3×3 matrix with differential algebra-valued elements, i.e. $M \in \mathrm{SO}_3\,(_nD_v)$ (whereas M would be in $\mathrm{SO}_3\,(\mathbb{R})$ in the linear case). The inverse spin transfer map is the inverse matrix $M^{-1} : X_{i+1} \to X_i$.

The time reversal results in the sign change of momentum (coordinates a and b) and the longitudinal offset (coordinate l) [5, p.147].

To obtain the reverse spin transfer map M^{R}, we apply the reversion transformation to the inverse spin transfer map:

$$M^{\mathrm{R}} = \hat{R}_{\mathrm{S}} \cdot (M^{-1} \circ \hat{R}) \cdot \hat{R}_{\mathrm{S}},$$

where

$$\hat{R} = \begin{pmatrix} 1 & 0 & 0 & 0 & 0 & 0 \\ 0 & 1 & 0 & 0 & 0 & 0 \\ 0 & 0 & 1 & 0 & 0 & 0 \\ 0 & 0 & 0 & -1 & 0 & 0 \\ 0 & 0 & 0 & 0 & -1 & 0 \\ 0 & 0 & 0 & 0 & 0 & -1 \end{pmatrix} \quad (1)$$

acts on the *COSY INFINITY* 6-dimensional phase space coordinates $(x, y, \delta_K, a, b, l)$ and

$$\hat{R}_{\mathrm{S}} = \begin{pmatrix} 1 & 0 & 0 \\ 0 & 1 & 0 \\ 0 & 0 & -1 \end{pmatrix} \quad (2)$$

acts on the spin vector coordinates (s_x, s_y, s_z).

D.   Error Field Implementation

According to the Thomas-BMT equation, a small perturbation of the magnetic field acts, to the first order, as a small rotation on the spin vector. We have implemented field errors as small, normally distributed spin kicks applied to the magnetic dipoles or combined E+B elements. The spin elements are interposed automatically into the *COSY INFINITY* code using one of the *Mathematica* notebooks.

III.   SPIN DECOHERENCE STUDY

In 2015, we studied the spin decoherence in the three *Senichev* lattices [3, 6]. We presented a summary of this

study at SPIN 2016 for reference and comprehensiveness purposes.

The primary findings were:

1. With an optimized sextupole family strength, the spin decoherence often remains in the same range for at least 5×10^5 turns. This is promising in respect to the requirement of maintaining a spin coherence time of no less than ~ 1000 seconds to possibly build a measurable EDM signal.

2. The QFS structure decoherence is at least as good as, or better than, the FS structure decoherence.

IV. SYSTEMATIC ERRORS STUDY

Systematic errors due to imperfections in the physical facility can create a fake EDM signal. Considering (1) the Thomas-BMT equation, (2) the reversal of the magnetic field in the reverse lattice, and (3) the lattice structure's imposition of an interdependence on the strengths of magnetic bends and electrostatic deflectors, we focus our attention on the rotational magnet misalignments.

We have studied the effect of rotational magnet misalignments on spin dynamics, namely spin decoherence and frequencies of rotation in a vertical plane, in QFS and FS structures. The error field components B_x and B_z are the most relevant to the detection of an EDM signal because the B_y component only results in differential rotation in the horizontal plane.

A. Clockwise and Counterclockwise Lattice Traversal

To extract the EDM signal, we propose to track polarized particle bunches in the QFS and FS lattices in both clockwise (CW) and counterclockwise (CCW) directions. We consider the CW direction to be forward and the CCW direction to be reverse. We use the fact that, in the linear approximation, the reverse spin transfer map coincides with the inverse spin transfer map. The reversal of a transfer map reverses the direction of the magnetic field but doesn't affect the electrostatic field.

B. B_x Error Field Component

An approximate solution of the Thomas-BMT equation in a magnetic dipole with an error field B_x and initial

conditions $\vec{S} = \vec{e}_z$ and $\Omega_z = 0$ is

$$S_x(t) = \frac{\Omega_y \sin\left(\sqrt{\Omega_x^2 + \Omega_y^2}\, t\right)}{\sqrt{\Omega_x^2 + \Omega_y^2}},$$

$$S_y(t) = -\frac{\Omega_x \sin\left(\sqrt{\Omega_x^2 + \Omega_y^2}\, t\right)}{\sqrt{\Omega_x^2 + \Omega_y^2}}.$$

The rotation frequencies are $\Omega_x^{\mathrm{CW}} = \Omega_{B_x}^{\mathrm{CW}} + \Omega_{\mathrm{EDM}}$ and $\Omega_x^{\mathrm{CCW}} = -\Omega_{B_x}^{\mathrm{CCW}} + \Omega_{\mathrm{EDM}}$ in the vertical plane and $\Omega_y = 0 + \langle \delta\Omega_{\mathrm{decoh}} \rangle$ in the horizontal plane.

It is necessary to (1) minimize the decoherence in the vertical plane $\sigma_{\Omega_{B_x}}$ the same way as in the horizontal plane using the RF cavity and sextupole families and (2) minimize $\left| \Omega_{B_x}^{\mathrm{CW}} - \Omega_{B_x}^{\mathrm{CCW}} \right|$ by calibrating the fields of the magnets using the spin precession frequency in the horizontal plane.

Rotation frequency due to EDM is obtained by $\Omega_{\mathrm{EDM}} = \left(\Omega_x^{\mathrm{CW}} + \Omega_x^{\mathrm{CCW}} \right) / 2$.

C. B_z Error Field Component

From an approximate solution of the Thomas-BMT equation in a magnetic dipole with an error field B_z, $\Omega_z = \Omega_{B_z}$, $\Omega_y = \langle \Omega_{\mathrm{decoh}} \rangle$, $\Omega_{B_z} \ll \langle \Omega_{\mathrm{decoh}} \rangle$, and initial conditions $\vec{S} = \vec{e}_z$ and $\Omega_x = 0$

$$\langle S_x(t) \rangle = \sin\left(\langle \Omega_{\mathrm{decoh}} \rangle t\right),$$

$$\langle S_y(t) \rangle = \frac{\Omega_{B_Z}}{\langle \Omega_{\mathrm{decoh}} \rangle} \left[1 - \cos\left(\langle \Omega_{\mathrm{decoh}} \rangle t\right)\right],$$

we see that the fake EDM signal has a factor of $\Omega_{B_z} / \langle \delta\Omega_{\mathrm{decoh}} \rangle$.

The method of error field component mitigation for B_x is not applicable to B_z.

We have to minimize Ω_{B_z} to $\sim 10^{-9}$ rad/sec using additional trim coils.

D. Outcome of the B_x and B_z Component Mitigation Method

With the application of the error component mitigation method outlined here, a realistic Fermi estimate of measurement accuracy for Ω_{EDM} is 10^{-4} to 10^{-5} rad/sec.

As a result, the accuracy of EDM signal measurement in one run is 10^{-24} to 10^{-25} e · cm.

The accuracy of the EDM signal measurement after one year of measurement may be 10^{-29} to 10^{-30} e · cm.

E. QFS/FS Conditions and Fringe Fields

Considering the error field components, we need to study the resulting spin dynamics and decoherence in

the vertical plane for the $E+B$ (QFS) and BNL (FS) lattices. We have designed the $E+B$ and BNL lattices to satisfy the QFS or FS condition respectively in the linear approximation. Taking into account the fringe fields, the QFS/FS condition is approximately satisfied, resulting in spin rotation in the horizontal plane. For the study of spin decoherence in the horizontal plane, this is not an issue, because in that case the spin decoherence is not significantly affected. However, when error field components result in spin decoherence in the vertical plane, the average spin direction in the horizontal plane affects, among other things, the magnitude of the spin motive force in the vertical plane. In the systematic errors study, we have to consider in detail whether the QFS/FS condition is satisfied exactly or approximately.

In a previous study, we had tried fitting the system configuration to satisfy the nonlinear QFS/FS condition. This worked quite well except that there was a small residual error in the measure of the condition. Although orbital motion must conserve energy and be symplectic, the requirement for spin motion is that the length of the spin vector is unity. We had recently introduced small spin kicks after each turn (effectively an infinitely thin dipole acting on spin) to address the issue. In real-life operations, the field strengths can be adjusted to satisfy the QFS/FS condition regarding the required precision.

F. Spikes in Horizontal Spin Decoherence Measure at Zenith and Nadir

With spin at the poles of the spherical coordinate system ($\theta = \pm\pi/2$), we may observe apparent spikes in the horizontal spin decoherence. This is not due to a physical effect, but rather to defining the measure of spin decoherence as σ_ϕ and σ_θ. To confirm this, we have analyzed a minimal test case with three particles in *Mathematica*. If we wished to avoid this effect, we could use an alternative measure of spin decoherence, such as $\sigma_{S_x^2+S_y^2}$ in the horizontal plane and $\sigma_{S_z^2}$ in the vertical plane. However, this alternative measure of spin decoherence has less physical sense for large spin decoherence than with σ_ϕ and σ_θ. The observed spikes in the horizontal spin decoherence measure can be trivially accounted for in the analysis, and their presence gives a useful visual indicator for spin motion in the vertical plane.

G. Spin-tracking Datasets

We have calculated more than 46 spin-tracking datasets in the systematic errors study. This includes: (1) *Senichev 6.3*, $E+B$, and BNL lattices; (2) optimization by SFP, SDP, SFP1, and SDP2 [7] sextupole families as well cases with no optimization; (3) $-0.5x$, $0x$, $0.05x$, $0.5x$, $1x$, and $2x$ corrective spin kicks, where $1x$ is defined to exactly satisfy the QFS/FS condition; and (4) magnet misalignment

angles of 10^{-4} rad and, for quality assurance purposes, 5×10^{-5} rad.

Each dataset consists of 24 *COSY* output files, including: (1) B_x and B_z error fields and no error field; (2) the CW and CCW lattice traversal directions; (3) tracking in the horizontal and the vertical plane, and (4) initial coordinates of the particle bunch distributed in x and δ_K.

H. Vertical Spin Decoherence, Approximate QFS/FS

See the plots in Fig. 1 for typical examples. With optimization by the SDP sextupoles, for the CW direction with error field components B_x (blue curve color) and B_z (green), the vertical spin decoherence grows to $\sim 10^{-6}$ rad for the $E+B$ lattice and $\sim 10^{-7.5}$ rad for the BNL lattice in 420 thousand turns. With optimization by the SDP sextupoles, for the CCW direction with error field components B_x (orange) and B_z (red), the vertical spin decoherence has the upper bound of $\sim 10^{-5}$ rad for the $E+B$ lattice and $\sim 10^{-6}$ rad for the BNL lattice in 420 thousand turns.

I. Vertical Spin Decoherence, Exact QFS/FS

See the plots in Fig. 2 for typical examples. With optimization by the SDP sextupoles, for the CW direction with error field components B_x (blue curve color) and B_z (green), the vertical spin decoherence has the upper bound of $\sim 10^{-5}$ rad for the $E+B$ lattice and $10^{-6.5}$ to 10^{-5} rad for the BNL lattice in 420 thousand turns. With optimization by the SDP sextupoles, for the CCW direction with error field components B_x (orange) and B_z (red), the vertical spin decoherence has the upper bound of $\sim 10^{-3}$ rad for the $E+B$ lattice and 10^{-4} to 10^{-3} rad for the BNL lattice in 420 thousand turns.

J. Summary of the Results

1. The spin decoherence in the vertical plane is proportional to the B_x and B_z error field components as expected.

2. When a spin kick is used for the exact QFS/FS, the vertical spin decoherence in both lattices is about 10 to 10^2 higher, partly due to the spin rotation in the horizontal plane that effectively acts as an oscillation factor in the vertical spin motive force component in case of inexact QFS/FS.

3. Because the sextupoles were optimized for the CW lattices, vertical spin decoherence is somewhat higher for the CCW direction.
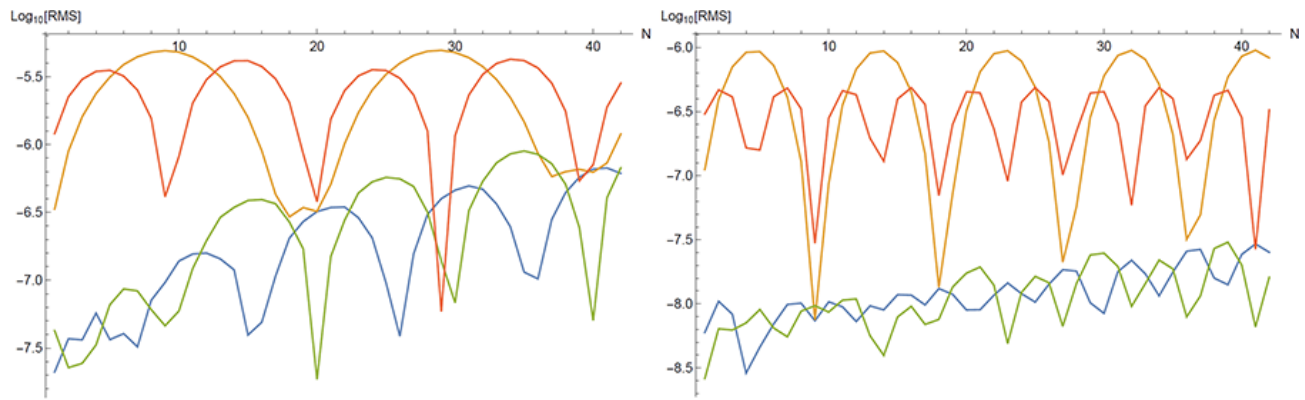
Figure 1. The vertical spin decoherence (as $\log_{10}$ (rms)) versus the number of turns (as $N = \text{turns}/1000$), $E+B$ lattice (left plot) and BNL lattice (right plot), optimization by the SDP sextupole family, and approximate QFS/FS (no corrective spin kick).
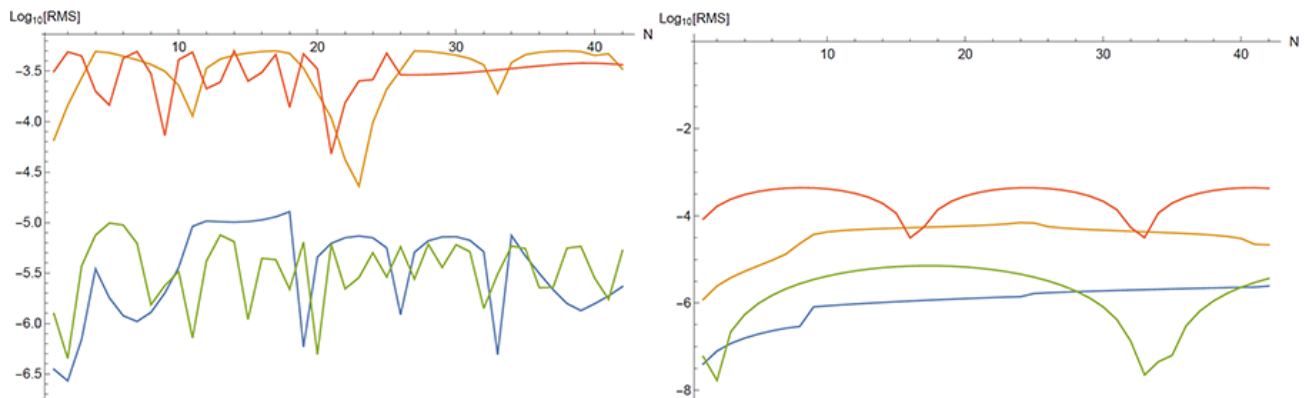

Figure 2. The vertical spin decoherence (as $\log_{10}$ (rms)) versus the number of turns (as $N = \text{turns}/1000$), $E+B$ lattice (left plot) and BNL lattice (right plot), optimization by the SDP sextupole family, exact QFS/FS ($1x$ corrective spin kick).

4. Some of the apparent periodic spikes in spin decoherence are due to the use of the spherical coordinate system for the spin decoherence measure.

5. With an optimized sextupole family strength and with exact QFS/FS (via corrective spin kick), the vertical spin decoherence due to systematic errors often remains in the same range for at least 5×10^5 turns in both the $E+B$ (QFS) and BNL (FS) lattices. The vertical spin decoherence in the $E+B$ (QFS) and BNL (FS) lattices is qualitatively very similar and quantitatively within about 1-2 orders.

V. CONCLUSION

1. We estimate that in one year of measurement, the accuracy of EDM signal measurement in QFS and FS lattices may be 10^{-29} to 10^{-30} e · cm.

2. For at least 5×10^5 turns, the spin decoherence data in the vertical plane due to error magnetic field components in the $E+B$ (QFS) and BNL (FS) lattices is:

(a) quantitatively within about 1–2 orders; and

(b) qualitatively without significant differences.

3. This systematic errors study is ongoing and will yield additional results.

4. In the context of the systematic errors study, we will study the vertical spin motion and spin decoherence with B_x and B_z error field components while:

(a) slightly varying and optimizing the QFS/FS condition measure through the electrostatic and magnetic field strengths; and

(b) tracking the particle bunches for a larger number of turns.

---

[1] Y. Senichev, A. Lehrach, B. Lorentz, R. Maier, S. Andrianov, A. Ivanov, S. Chekmenev, M. Berz, and E. Valetov (on behalf of the JEDI Collaboration), in *Proceedings of IPAC 2015, Richmond, VA* (2015) MOPWA044.

[2] D. Anastassopoulos *et al.*, "AGS proposal: Search for a permanent electric dipole moment of the deuteron nucleus at the 10-29 e Â· cm level," BNL Report, Brookhaven National Laboratory, U.S.A. (2008), goo.gl/1K1TNq.

[3] Y. Senichev, M. Berz, E. Valetov, S. Chekmenev, S. Andrianov, and A. Ivanov (on behalf of the JEDI Collaboration), in *Proceedings of ICAP 2015, Shanghai, China* (2015) MODBC4.

[4] K. Makino and M. Berz, Nuclear Instruments and Methods in Physics Research, Section A: Accelerators, Spectrometers, Detectors and Associated Equipment **558**, 346 (2006).

[5] M. Berz, *Modern map methods in particle beam physics*, Advances in Imaging and Electron Physics (Academic Press, San Diego, CA, 1999).

[6] E. Valetov, M. Berz, and Y. Senichev (on behalf of the JEDI Collaboration), in *Proceedings of ICAP 2015, Shanghai, China* (2015) THDBC2.

[7] In sextupole family names, 'F' denotes focusing, 'D' defocusing, 'P' positive dispersion, and 'N' negative dispersion. The *BNL* lattice only has positive dispersion sextupole families.

[8] Y. Senichev, S. Andrianov, M. Berz, S. Chekmenev, A. Ivanov, B. Lorentz, J. Pretz, and E. Valetov (on behalf of the JEDI Collaboration), in *Proceedings of IPAC 2016, Busan, Korea* (2016) THPMR005.